nature nanotechnology

SUPPLEMENTARY INFORMATION

DOI: 10.1038/NNANO.2010.248

Single-Walled Carbon Nanotubes as Excitonic Optical Wires

Daniel Y. Joh[1,2]*, Jesse Kinder[2]*, Lihong H. Herman[1]*, Sang-Yong Ju[2], Michael A. Segal[2], Jeffreys N. Johnson[2], Garnet K.-L. Chan[2], and Jiwoong Park[2,3†]

*These authors contributed equally to this work

†To whom correspondence should be addressed. Email: jpark@cornell.edu

DOI: 10.1038/NNANO.2010.248

Supplementary Information Contents

Experimental Apparatus for On-Chip Rayleigh Imaging

Aligned SWNTs were grown on a quartz substrate following a procedure adapted from Kocabas *et al*. (*Small*, **1**, 1110 (2005)). A tuneable wavelength laser beam is linearly polarized and introduced into an index-matched sample geometry at an angle using a darkfield condenser (DCW), and is reflected completely by total internal reflection at the uppermost glass/air interface and subsequently directed back down through the condenser. This geometry prevents the excitation laser from entering the detection optics. The light scattered from SWNTs is collected by an objective lens (OL) (UIS2 PlanSAPO 40x, N.A. 0.95) and focused onto a CCD camera by the tube lens (TL). For further details, see reference 27 of the main text.

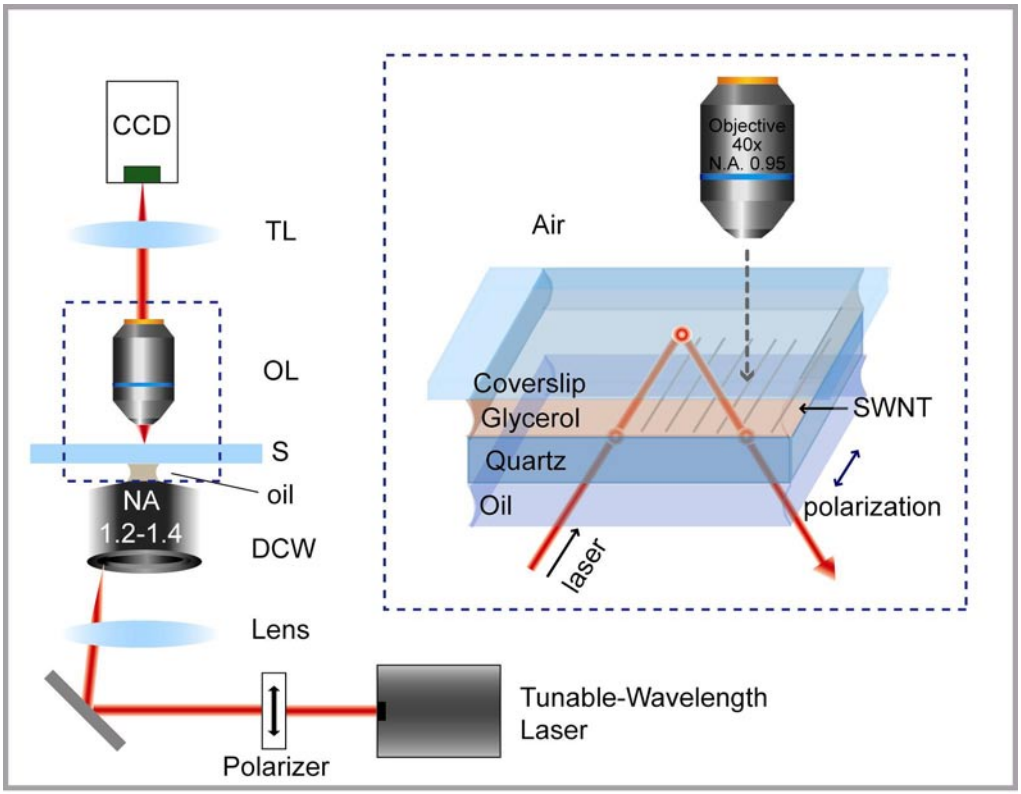

Figure S1. On-chip Rayleigh imaging setup. See text above for abbreviations.

DOI: 10.1038/NNANO.2010.248

Measuring Spatial Distribution of Scattered Light (Fraunhofer Imaging)

Fig. S2 describes the experimental geometry used to measure the spatial distribution of the scattered light from individual SWNTs. The scattered light was collected by a high numerical aperture (N.A. = 0.95) objective lens (OL). An iris was placed at the image forming plane of the tube lens (TL) to observe only one SWNT at a time and then an additional lens was used to collect the spatial distribution of scattered light from the same SWNT, which was imaged using a CCD camera.

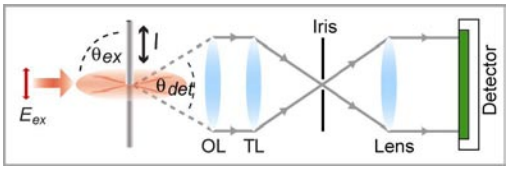

Figure S2: Schematic of SWNT Fraunhofer imaging. See text above for abbreviations.

Polarization Dependence

The Rayleigh scattering amplitude for SWNTs is strongly polarization dependent, reaching a maximum when the electric field is polarized parallel to the nanotube axis. This effect was demonstrated in previous Rayleigh scattering experiments (*Science*, **306**, 1540 (2004)), and we show polarization-dependent behavior in Fig. S3 that is consistent with these previous measurements. In Fig. S3 we show optical images of a SWNT in which the polarization of the excitation laser (P_{ex}) and that of an analyzer placed after the objective lens (P_{det}) are parallel (||) and/or perpendicular ($\perp$) to the nanotube axis. The data show that the nanotube is only visible when both P_{ex} and P_{det} are parallel to the SWNT axis.

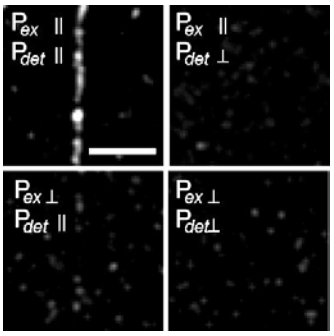

Figure S3: Polarization dependence for SWNT Rayleigh scattering. See text above for abbreviations. Scale bar 4, μm.

Spectral response for bent SWNTs

In this section, we show how the spectral response for SWNTs is mainly controlled by the intrinsic properties of the material, while the spatial propagation of the scattered field is independently determined by their shape. Fig. S4a shows an AFM image of an initially straight SWNT that eventually curves along its length. By recording Rayleigh spectra in curved and straight regions (sample spectra shown in Fig. S4d), we observe similar wavelength dependence along the length of the nanotube.

DOI: 10.1038/NNANO.2010.248

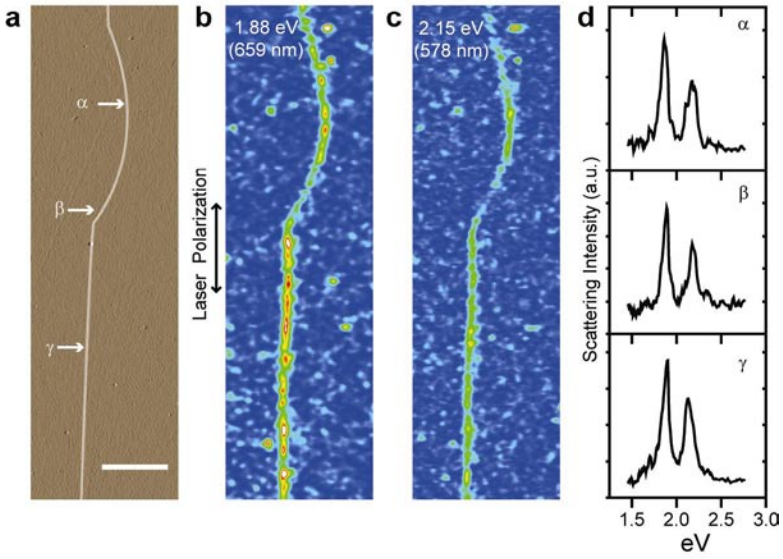

Figure S4: Optical scattering from curved *vs.* straight regions of an isolated SWNT. **a,** AFM image of the SWNT (nanotube highlighted in white for clarity). Scale bar, 5 μm. **b, c,** Corresponding Rayleigh images taken at 1.88 eV (**b**) and 2.15 eV (**c**). **d,** Rayleigh spectra recorded at the locations marked by Greek symbols in (**a**).

Although generally we observe uniform wavelength-dependence for this nanotube in both straight and curved regions, a closer look at spatial profiles (Figs. S4b and S4c) of the measured Rayleigh scattering *intensity* (at resonance) reveals distinct *orientation*-dependence (*i.e.* θ_{ex} dependence); for instance, the measured Rayleigh scattering intensity for curved region β is lower than that of straight region γ for both resonances at 1.88 eV and 2.15 eV. We attribute this decrease in intensity to two major factors: 1) polarization-dependent scattering and 2) radiation directivity.

To further illustrate this point, we first show the AFM image of a different nanotube (d_{AFM} = 1.46 nm) that bends much more sharply along its length (Fig. S5a) than

the SWNT shown in Fig S4. Fig. S5b spatially maps the measured Rayleigh scattering intensity. The optical signal of the SWNT is brightest in regions where θ_{ex} = 90° and disappears completely in the middle region where $\theta_{ex} \neq 90°$. Since the polarization-dependent scattering amplitude of SWNTs is proportional to $\cos^2(90° - \theta_{ex})$, this predicts that the SWNT's optical intensity in the outlined region should be approximately one-half that of the bright regions, which is not observed. The further reduction of the optical signal in the outlined region can be attributed to the directed radiation pattern of SWNTs: when θ_{ex} is much steeper than 90°, the resulting radiation cone may lie outside of the detection angle of our optics (Fig. S5e).

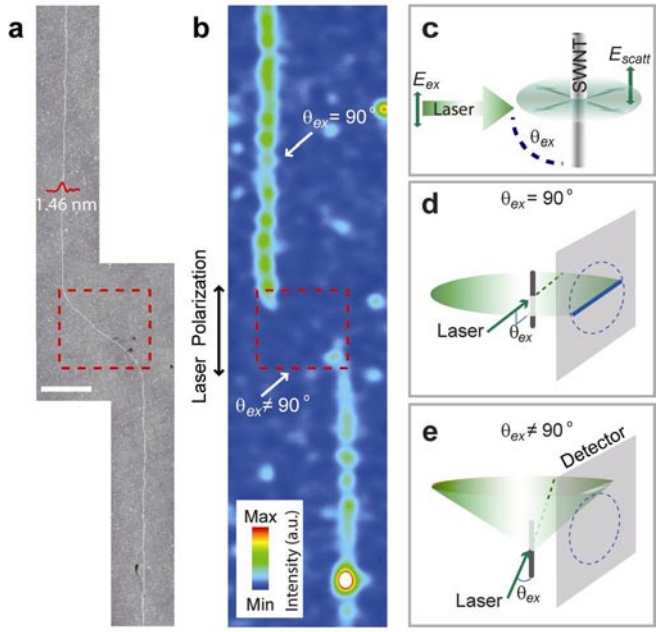

Figure S5: Radiation directivity dependence of the observed Rayleigh scattering intensity. **a, b,** Composite AFM image (**a**) and optical image (**b**) of the SWNT, with the bent region outlined in red. Scale bar, 2 μm. **c,** Laser excitation geometry of SWNTs **d, e,** Direction-dependent scattering of SWNTs. When θ_{ex}

DOI: 10.1038/NNANO.2010.248

becomes much different than 90°, the radiation cone may lie outside of our detection optics (e).

Patterning SWNTs with a Laser

The Rayleigh images of the sample containing aligned SWNTs were first obtained to locate the nanotubes before any cutting was performed. Next, high-intensity supercontuum light (NKT Photonics, Koheras SuperK Compact) was focused onto the sample plane (glycerol-quartz interface) after passing through a wideband hot mirror (W) (Thorlabs FM01) such that the peak laser pulse power after hot mirror is ~420 W. The stage was then raster-scanned in the x-y plane to pattern the tubes into periodic segments as shown in Fig. 2.

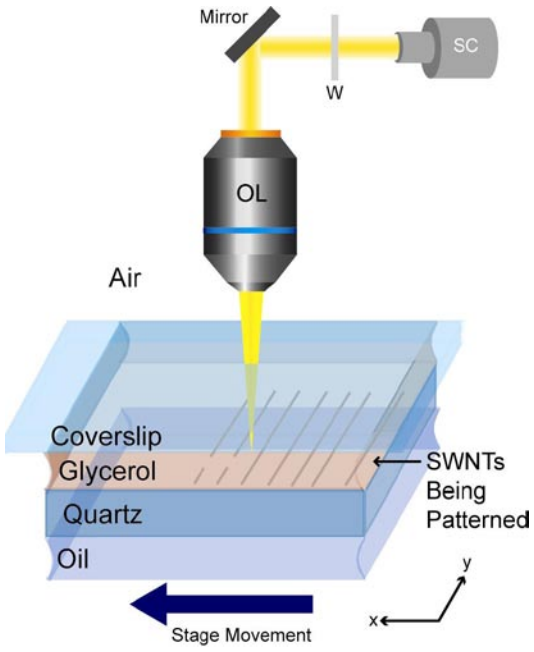

Figure S6: Schematic for laser-induced cutting of SWNTs. See text above for abbreviations.

Derivation of Equation (1)

For an infinite straight wire, the total radiated power per unit length (P_{rad}) averaged over time is given by $P_{rad} = \frac{1}{8} Zk \mid I(\omega) \mid^2$, where $I(\omega)$ is the surface current (Abbott, T. A. & Griffiths, D. J. *Am. J. Phys.* **53**, 1203-1211 (1985), ref [29]). Furthermore, if the incident beam has an electric field $E(\omega) = \left|E_o\right| e^{-i\omega t}$, the total scattered light power is $P_{scatt} = \frac{1}{2} \delta_{scatt} \mid E_0 \mid^2 Z^{-1}$. In this regime, the two expressions for power are equivalent. Equating the two expressions for power yields $\delta_{scatt} = \frac{1}{2} \pi^3 Z^2 \mid \sigma(\omega) \mid^2 d_{NT}^2 \lambda^{-1}$. This expression is consistent with Bachilo, S. *et al. Science* **298**, 2361-2366 (2002), ref [12], except for its dependence on nanotube diameter: this is due to our treatment of nanotubes as long hollow cylinders (or wires), instead of long solid cylinders.

Chiral Index Assignments for SWNTs in Figure 3c and Figure 4

For SWNTs shown in Figs. 3c & 4, we provide a table of possible (*n*, *m*) assignments based on Rayleigh scattering and AFM measurements. We assigned unique (*n*, *m*) values for about half of the SWNTs studied, while for the other half they were narrowed down to two or more possible indices due to the high density of optical resonances for larger diameter nanotubes. The labels for data points in Fig. S7, which is identical to Fig. 3c except for the labels, correspond to those in Table S1. The possible structural (*n*, *m*) index assignments for the SWNTs in Fig. 4 are indicated by *L* and *R* at the end of the table.

DOI: 10.1038/NNANO.2010.248

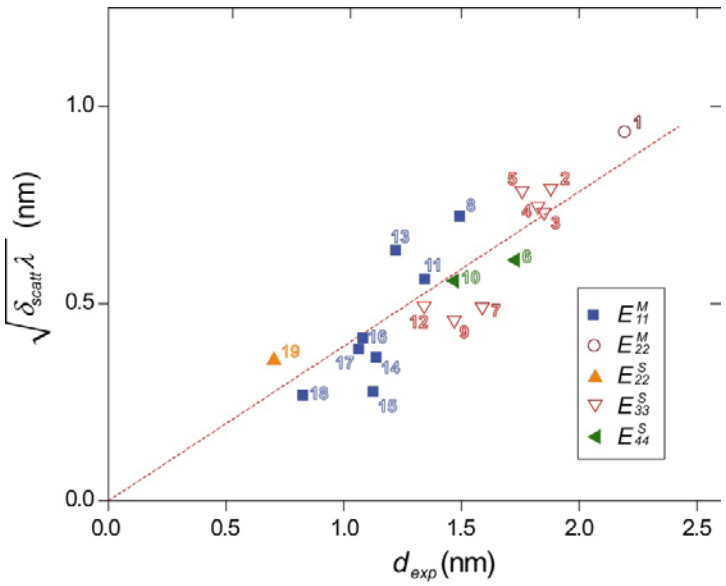

Figure S7: Data points from Fig. 3c with labels corresponding to those in Table S1.

Tube number	Diameters (nm)	Resonant Energy (eV)	Transition	Possible (*n*, *m*) values
Fig. 3c				
1	2.19	2.163	E_{22}^{M}	(24, 6) (19, 13)
2	1.88	1.873	E_{33}^{S}	(14, 13)
3	1.85	1.950	E_{33}^{S}	(16 ,11)
4	1.82	2.147	E_{33}^{S}	More than two assignments
5	1.76	2.102	E_{33}^{S}	(21, 1) (20, 3)
6	1.73	2.174	E_{44}^{S}	(19, 5)
7	1.59	2.098	E_{33}^{S}	(15, 7)
8	1.49	1.869	E_{11}^{M}	(18, 0) (17, 2)
9	1.47	2.103	E_{33}^{S}	(15, 7) (16, 5)
10	1.47	2.412	E_{44}^{S}	(15, 7) (16, 5)
11	1.34	1.847	E_{11}^{M}	(15,3)
12	1.34	2.352	E_{33}^{S}	(13, 6)
13	1.22	2.155	E_{11}^{M}	More than two assignments
14	1.14	2.103	E_{11}^{M}	More than two assignments
15	1.12	2.214	E_{11}^{M}	(8, 8) (11, 5)
16	1.08	2.326	E_{11}^{M}	(9, 6)
17	1.06	2.342	E_{11}^{M}	(12, 3)
18	0.83	2.331	E_{11}^{M}	(10, 1) (9, 3)
19	0.70	2.211	E_{22}^{S}	(6, 4)
Fig. 4				
L	1.75	1.95	E_{33}^{S}	(18, 7)
R	1.35	1.86	E_{11}^{M}	(14, 5) (11, 8)

Table S1: SWNT diameters (d_{exp}), experimentally determined resonant energies, electronic transition, and possible (n, m) values corresponding to the data points shown in Fig. S7. The last two rows show the same information for the SWNTs in Fig. 4 of the main text.

Measurement of scattering cross section width on SWNT resonance

The scattering cross section width of an individual SWNT was measured by first identifying its resonance wavelength from its Rayleigh spectrum. In our setup, the light scattered by a SWNT is detected with a detection angle (θ_{det}) of 80.6 out of 360 degrees. Thus, the total scattering detection efficiency in our setup is given by (80.6/360) $\times T_{OE}(\lambda)\times QE_{CCD}(\lambda)$, where T_{OE} is the combined transmission efficiency of all optical elements and QE_{CCD} the quantum efficiency of the CCD, both measured at the resonance wavelength, λ. This enabled us to calculate the resonance scattering intensity ($I_{scatt,}$ [number of photons/um×sec]*)* per unit length of the SWNT. We then determined the power density per unit area of the excitation laser at the SWNT position ($I_{laser,}$ number of photons/um^2×sec]*)* by fitting the illumination profile to a 2D Gaussian. Dividing I_{scatt} by I_{laser} yields the scattering cross section width, δ_{scatt}.

Models for Dynamic Conductivity and Radiative Coupling of SWNTs

Here we will briefly describe the method used to calculate the conductivity data in Fig. 3. Our starting point is the Kubo formula for the conductivity:

$$\sigma(\omega) = \frac{\hbar}{i2\pi RL}\sum_{\alpha}\frac{|\langle\alpha|\mathbf{J}|\Omega\rangle|^2}{E_\alpha}\frac{2(\hbar\omega)}{E_\alpha^2-(\hbar\omega+i\hbar\gamma_\alpha)^2}.$$

DOI: 10.1038/NNANO.2010.248

$|\Omega\rangle$ indicates the ground state, $|\alpha\rangle$ is an excited state, E_α is the energy of the excitation, γ_α is the width of the excitation, R is the nanotube radius, L is the length of the tube, and ω is the frequency of the laser.

The low energy properties of carbon nanotubes can be calculated from an effective Dirac Hamiltonian (*Phys. Rev. Lett.*, **78**, 1932 (1997)). Imposing periodic boundary conditions on the linear $\mathbf{k}\cdot\mathbf{p}$ approximation to the tight-binding model near the K and K' points of graphene generates a series of hyperbolic bands with the dispersion relation

$$E(k) = (\hbar v_F / R)\sqrt{\Delta_n^2 + (kR)^2}$$

where $v_F \approx c/300$ is the Fermi velocity. The band gaps are $2\Delta_n(\hbar v_F / R)$ with $\Delta_n = n + \Delta_o$. n is an integer, and $\Delta_o = 0$ for metallic nanotubes (giving rise to a linear band for $n = 0$) and $\Delta_o = \pm 1/3$ in semiconducting nanotubes. Each band is 4-fold degenerate: a factor of 2 for spin and an additional factor of 2 for the degenerate K and K' points.

$E_o = \hbar v_F / R$ defines a natural energy scale for the nanotube. E_o also defines an effective mass: $m^* v_F^2 = E_o$, so that $m^* = \hbar / v_F R$.

With these definitions, the Kubo formula can be expressed in terms of a dimensionless oscillator strength:

$$f_\alpha = m^* \frac{|\langle \alpha | v_z | \Omega \rangle|^2}{E_\alpha},$$

The expression for the conductivity becomes

$$\sigma(\omega) = \frac{\hbar}{i2\pi RL} \cdot \frac{e^2}{m^*} \sum_\alpha f_\alpha \frac{2(\hbar\omega)}{E_\alpha^2 - (\hbar\omega + i\hbar\gamma_\alpha)^2}.$$

The optical properties of carbon nanotubes are strongly influenced by electron interactions. The Coulomb interaction leads to a large self energy that increases the transport gap. It also leads to the formation of strongly bound electron-hole pairs – excitons – below the band edge. Most of the spectral weight of an absorption or scattering peak is localized in a single exciton transition.

We calculated the exciton wave functions and energies using a model first developed by Ando (*J. Phys. Soc. Jpn*. **66**, 1066 (1997)). In this model, the free electron and hole energies and wave functions are calculated using the effective Dirac Hamiltonian. We modified the Dirac Hamiltonian to include trigonal warping effects near the band edge. These energies and wave functions are used to calculate the polarization and static dielectric function within the random phase approximation, which leads to a screened Coulomb interaction $V(k)$. The electron and hole self energies, $\Sigma_e(k)$ and $\Sigma_h(k)$, are calculated within the screened Hartree Fock approximation. The exciton wave functions and energies are obtained as solutions of a Bethe Salpeter equation:

$$E_\alpha \psi_\alpha(k) = [\varepsilon_p(k) + \Sigma_p(k) - \varepsilon_h(k) - \Sigma_h(k)]\psi_\alpha(k) + \sum_q V(q)\psi_\alpha(k+q)$$

We solved this equation in a two-band model. This is a good approximation for excitons in the lowest band of a semiconductor (E_{11}^S), but excitons in higher bands can dissociate into unbound electron-hole pairs in lower bands. This gives the exciton a finite lifetime, which we calculate using the golden rule following Kane and Mele (*Phys. Rev. Lett.* **90**, 207401 (2003)). Since the experiments were performed in glycerol ($n \approx 1.46$), we used a static dielectric constant of $\kappa = n^2 = 2.1$ to account for static screening of the

DOI: 10.1038/NNANO.2010.248

Coulomb interaction. RPA screening roughly doubles this value and leads to an exciton self energy of $\hbar\gamma \approx 0.05E_{\mathrm{o}}$ for all excitons. This is several orders of magnitude larger than the line width due to radiative recombination, so we ignore the latter.

To obtain the data in Fig. 3, we used the calculated exciton wave functions, energies, and lifetimes in the Kubo formula for the conductivity.

A. Peak Conductivity

The exciton model predicts a peak conductivity that is independent of the nanotube diameter. This can be inferred from the Kubo formula when a large fraction of the oscillator strength is concentrated in a single transition, as is the case for excitons in carbon nanotubes. The oscillator strength in the Dirac model of noninteracting electrons satisfies a sum rule:

$$\sum_{\alpha} f_{\alpha} = \frac{L}{2\pi R}$$

Using this sum rule, the conductivity may be expressed as

$$\sigma(\omega) = \frac{\hbar}{i(2\pi R)^2} \cdot \frac{e^2}{m^*} \frac{1}{E_{\mathrm{o}}} \sum_{\alpha} \phi_{\alpha} \frac{2(\hbar\omega)\cdot E_{\mathrm{o}}}{E_{\alpha}^2 - (\hbar\omega + i\hbar\gamma_{\alpha})^2},$$

where $\phi_{\alpha} = f_{\alpha} \Big/ \sum_{a} f_{\alpha}$ is the fraction of the total oscillator strength in the transition to $|\alpha\rangle$.

The sum is a dimensionless number and the prefactor sets the scale of the AC conductivity. Using the definitions of E_{o} and m^* given above, the conductivity is

$$\sigma(\omega) = \frac{e^2}{h} \cdot \frac{1}{2\pi i} \cdot \sum_{\alpha} \phi_{\alpha} \frac{2(\hbar\omega)\cdot E_{\mathrm{o}}}{E_{\alpha}^2 - (\hbar\omega + i\hbar\gamma_{\alpha})^2}.$$

We can place an upper bound on the conductivity by assuming all of the oscillator strength is concentrated in a single transition: $\phi_\alpha = \delta_{\alpha X}$. This is a good approximation to the exciton model, where $\phi_x \approx 0.6 - 0.8$, and the lowest exciton peak is well separated in energy from the rest of the spectrum. In this case,

$$\sigma(\omega) = \frac{e^2}{h} \cdot \frac{1}{2\pi i} \cdot \frac{2(\hbar\omega) \cdot E_o}{E_X^2 - (\hbar\omega + i\hbar\gamma_X)^2},$$

and the conductivity on resonance is

$$\sigma_P = \frac{e^2}{h} \cdot \frac{E_o}{2\pi\hbar\gamma_X} = \frac{e^2}{h} \cdot \frac{v_F \tau_X}{2\pi R}$$

If the exciton lifetime τ_X is proportional to the nanotube radius, then the peak conductivity will be independent of the radius.

Using the exciton linewidth due to dissociation into free electrons and holes ($\hbar\gamma_X \approx 0.05 E_o$) gives an upper limit on the peak conductivity of $\sigma_P \approx 3.2e^2/h$ per exciton.

The model also predicts that the peak conductivities in some metallic nanotubes should be roughly twice as large as those in semiconducting nanotubes. The $n = \pm 1$ bands in a metallic armchair nanotube are degenerate. In chiral nanotubes, trigonal warping lifts the degeneracy so that individual peaks can be resolved. The data show little difference in the peak conductivity between semiconducting and metallic nanotubes, which suggests that all five of the metallic nanotubes in the sample were chiral where the two slightly shifted resonances were unresolved, and thus form a single peak with its height similar to the uniform value 8 e^2/h in the range of wavelengths probed in the experiment. We expect

DOI: 10.1038/NNANO.2010.248

a wider range of peak conductivities in samples containing metallic nanotubes of all chiralities.

While other optical experiments have demonstrated the necessity of an exciton picture of the excitations, a peak conductivity that is independent of the nanotube radius is not specific to the exciton model here. We have calculated the peak conductivity in a free particle model with a constant scattering rate and a free particle model with acoustic phonon scattering, models in which the oscillator strength is not concentrated in a single transition. The peak conductivity is independent of the radius as long as the lifetime is inversely proportional to the nanotube radius. (This will be described elsewhere.)

B. Radiative Coupling

Fig. 4 shows a strong radiative coupling between two parallel nanotubes with similar Rayleigh spectra. As the laser frequency shifts from one resonance to the other, there is a large transfer of spectral weight between the nanotubes. A classical model of two parallel conducting wires can reproduce the qualitative features of this crossover. However, the experimental values of the conductivity are too small to induce a detectable effect. This suggests that a theory of correlated local fluctuations is necessary to fully understand the mechanism responsible for the abrupt transition observed in the experiment. Here we describe the radiative coupling between two parallel wires with overlapping resonances.

The vector potential $\mathbf{r}$ due to an arbitrary current density $\mathbf{J}(\mathbf{x})$ is

$$\mathbf{A}(\mathbf{r}) = \frac{1}{c}\int d\mathbf{x}\,\frac{e^{ik|\mathbf{r}-\mathbf{x}|}}{|\mathbf{r}-\mathbf{x}|}\mathbf{J}(\mathbf{x})$$

and the radiated field at **r** is $\mathbf{E}(\mathbf{r}) = (1/k)\nabla\times\nabla\times\mathbf{A}(\mathbf{r})$. We consider an infinite wire with conductivity $\sigma(\omega)$ driven by an oscillating field $E_0(\omega)$ applied along its axis. The field induces a uniform surface current $I(\omega) = 2\pi R\sigma(\omega)E_0(\omega)$. The scattered field at a point distance D away from the wire is parallel to the applied field:

$$E_S(\omega) = \frac{i}{\omega}2\pi R\frac{1}{D^2}\sigma(\omega)\beta(kD)E_0(\omega)$$

where $\beta(kD)$ is a dimensionless geometric factor obtained by integrating along the length of the wire:

$$\beta(kD) = \int_{-\infty}^{\infty} dx\left(\frac{2}{(1+x^2)^{5/2}} - \frac{2ikD}{(1+x^2)^2} - \frac{k^2D^2}{(1+x^2)^{3/2}}\right)e^{ikD\sqrt{1+x^2}}$$

The scattered field is proportional to the applied field: $E_S(\omega) = \alpha(\omega)E_0(\omega)$.

If two parallel wires A and B are driven by the same applied field, then the electric field at one wire is a superposition of the applied field and the scattered field of the other wire. This leads to a set of coupled equations:

$$E_A(\omega) = \alpha_A(\omega)[E_0(\omega) + E_B(\omega)]$$

$$E_B(\omega) = \alpha_B(\omega)[E_0(\omega)e^{i\varphi} + E_A(\omega)],$$

where φ accounts for the phase difference in the applied field between the two wires. For instance, if the light is incident on the plane of the two wires at angle θ, then $\varphi = kd\sin\theta$. The scattered fields are

$$E_A(\omega) = \frac{1+e^{i\varphi}\alpha_B(\omega)}{1-\alpha_A(\omega)\alpha_B(\omega)}\alpha_A(\omega)E_0(\omega)$$

$$E_B(\omega) = \frac{1+e^{-i\varphi}\alpha_A(\omega)}{1-\alpha_A(\omega)\alpha_B(\omega)}\alpha_B(\omega)E_0(\omega)$$

DOI: 10.1038/NNANO.2010.248

The scattered fields are affected by many different phases: the geometric phase from $\beta(kD)$, the phase due to the angle of incidence of the driving field, and the phase of the conductivity as the frequency of the applied field passes through a resonance. When $|\alpha_{A,B}(\omega)| \ll 1$, the scattered fields are those of independent wires. However, when $|\alpha_{A,B}(\omega)| \sim 1$, the scattered field of a wire is strongly affected by that of the other wire. For the wires in Fig. 4, $\lambda \approx 650$ nm, $D \approx 300$ nm, and $kD \approx 3$. The geometric factor $\beta(kD)$ is on the order of 1, so the coupling strength is determined by the conductivity. For a peak conductivity of 10 e^2/h,

$$\alpha(\omega) \approx 10 \frac{e^2}{\hbar\omega} \frac{R}{D^2} \approx 10^{-5}$$

This is much too small to modify the scattered fields when two wires run parallel to one another, and shows that a mean field description of the scattered fields cannot explain the observed coupling. The simple mean field description of light scattering used to calculate the conductivity, which correctly describes the optical scattering properties of single nanotubes, ignores effects such as spatial and temporal fluctuations in the surface currents and correlations between the two nanotubes. The size of the surface currents required to reproduce the qualitative features of Fig. 4 suggests that large fluctuations on short length and time scales may be responsible for the strong radiative coupling. Since there is currently no theoretical model for these effects, we treated the effective conductivity as a free parameter in analyzing the data. If the surface currents are enhanced by a factor of 1000, it is possible to reproduce the qualitative features of the sharp transition in Fig. 4. The parameters used to generate the plot were $D = 300$ nm, $n = 1.47$, $E_A = 1.85$ eV, $E_B = 1.98$ eV, $\Gamma_A = 0.12$ eV, $\Gamma_B = 0.15$ eV, and $\sin\theta = 1.33/1.47$.